

## Detection of Neurotransmitter (Levodopa) in Vegetables Using Nitrogen-Doped Graphene Oxide Incorporated Nickel Oxide Modified Electrode

Vengudusamy Renganathan<sup>1#</sup>, Ragu Sasikumar<sup>1#</sup>, Shen-Ming Chen<sup>1,\*</sup>, Tse-Wei Chen<sup>1</sup>, Syang-Peng Rwei<sup>2</sup>, Shih-Yi Lee<sup>3,\*</sup>, Wen-Han Chang<sup>4,5,6</sup>, Bih-Show Lou<sup>7,8\*</sup>,

<sup>1</sup> Department of Chemical Engineering and Biotechnology, National Taipei University of Technology, Taiwan.

<sup>2</sup> Institute of Organic and Polymeric Materials, National Taipei University of Technology, Taiwan

<sup>3</sup> Division of Pulmonary and Critical Care Medicine, MacKay Memorial Hospital; MacKay Junior College of Medicine, Nursing, and Management, Taipei, Taiwan

<sup>4</sup> Department of Medicine, MacKay Medical College, Taipei, Taiwan <sup>5</sup> Department of Emergency Medicine, MacKay Memorial Hospital; Institute of Mechatronic Engineering; Institute of Manufacturing Technology and Department of Mechanical Engineering, National Taipei University of Technology, Taipei, Taiwan; <sup>6</sup> Graduate Institute of Injury Prevention and Control; School of Medicine, Taipei Medical University, Taipei, Taiwan

<sup>7</sup> Chemistry Division, Center for General Education, Chang Gung University, Taoyuan, Taiwan,

<sup>8</sup> Department of Nuclear Medicine and Molecular Imaging Center, Chang Gung Memorial Hospital, Taoyuan, Taiwan

# Authors contributed equally

\*E-mail: [smchen78@ms15.hinet.net](mailto:smchen78@ms15.hinet.net), [leesyi5538@yahoo.com.tw](mailto:leesyi5538@yahoo.com.tw), [blou@mail.cgu.edu.tw](mailto:blou@mail.cgu.edu.tw)

Received: 23 March 2018 / Accepted: 7 May 2018 / Published: 5 June 2018

---

Nitrogen-doped graphene supported with Nickel oxide (N-GE/NiO) nanocomposite were prepared to develop the sensor for determination of L-dopa. The structure and morphology of the N-GE/NiO nanocomposite was characterized by powder X-ray diffraction (PXRD), Fourier transform Infra-red (FT-IR), Raman spectroscopy, thermogravimetric analysis (TGA), field emission scanning electron microscopy (FE-SEM), transmission electron microscopy (TEM) and the electrochemical response of L-dopa was also studied by cyclic voltammetry (CV) and differential pulse voltammetry (DPV) in phosphate buffer solution (PBS) at pH 7.0. The experimental results recommended that N-GE/NiO nanocomposite electro-oxidation response is greater than that of the bare electrode. The DPV results reports of L-dopa were increased linearly in the range from 0.03 – 386.8  $\mu\text{M}$  with a limit of detection is about 17 nM. Finally, the proposed sensor was applied for the sensitive determination of L-dopa in the vegetable sample and the achieved results were relatively promising.

---

**Keywords:** Graphene oxide, Nickel oxide, L-dopa, cyclic voltammetry, sweet potato.

## 1. INTRODUCTION

Carbon and carbon-based materials like graphene (GE), graphene oxide (GO) and carbon nanotubes (CNTs) have excellent properties owing to its surface area and conductivity. Among these a two-dimensional carbon network, GE has been highly attractive, due to the exclusive structural and physiochemical properties [1]. These carbon bonds are  $sp^2$  hybridized, and  $\sigma_{c-c}$  bond is one of the strongest bonds in materials and the  $\pi$  bond is only accountable for the electron conduction of GE, providing the weak interaction among GE layers or between GE and substrate [2]. This electron configuration is the origin to the large surface area of GE ( $2630 \text{ m}^2 \text{ g}^{-1}$ ), which is higher than that of CNT ( $1315 \text{ m}^2 \text{ g}^{-1}$ ) and graphite ( $10 \text{ m}^2 \text{ g}^{-1}$ ) high electrical conductivity, which is 60-fold greater than single-walled carbon nanotubes (SWCNT), high mechanical strength (200 times greater than steel) and six orders of magnitude upper than copper and thermal conductivity and high elasticity [3, 4].

These excellent properties suggest for many possible applications such as energy storage, biosensors, electronics, and catalysis owing to its superior electrical conductivity and high specific surface area. In many cases, GE is prepared from the reduction of GO, which is helpful to possess the carboxylate (-COOH) and hydroxyl (-OH) functional groups in the structure. These functional groups of GE make a way to interact with metal oxides. However, during the reduction process of GO, the GE sheets lean towards irreversible agglomeration and the graphitic structure of GE is also damaged [5-7], which is going to decrease the electro-catalytic property of GE. In this case, the introduction of nitrogen (N) into GE when reduction process it may prevent the aggregation and enhance the reactivity and electron conductivity of GE. This is due to the formation of conjugation between  $sp^2$  hybridized carbon atoms and to the lone pair electrons of the nitrogen atom. Moreover, N-GE offers many binding sites as well as the improved sensitivity and biocompatibility in sensor application [8-10]. Various transition metal oxides such as NiO,  $\text{Co}_3\text{O}_4$ , CuO,  $\text{RuO}_2$ , and NiO have been used for the electrochemical sensing applications. Among these metal oxides, NiO has good electrical conductive nature, distinct electro-activity, low of a cost, high stability which makes them suitable for electrochemical sensing applications. In current years, lots of NiO-based biosensors have been reported, in which the electrode surface treatment of NiO is initiated the vital for effective and fast electrochemical performance, due to the nanostructured NiO resources with a high surface area. Recent improvements in electrochemical sensor methods have also revealed that the electro-catalytic movement can be considerably improved by moving from bulk materials to nano-sized structures [11-15].

Levodopa ( $\text{C}_9\text{H}_{11}\text{NO}_4$ , L-dopa Scheme. 1) or L-3,4-dihydroxyphenylalanine medication used to most commonly prescribed for Parkinson's disease. This type of disease is associated with the loss of dopamine in the brain cell. L-dopa has entered the central nervous system (CNS), it is turned into dopamine by L-aromatic amino acid decarboxylase and increase the concentration of the chemicals in the treatment of Parkinson's disease [16]. L-dopa itself is an endogenous neurotransmitter, neuromodulator and both in the CNS in action of dopamine [17]. Dopamine has quickly to respond dystonia and it is used to the best treat the symptoms of the condition, particularly stiffness, tremors, and spasms control of Parkinson's disease. Therefore, determinations of its concentration in L-dopa different analytical methods have been developed such as high-performance liquid chromatography

[18], fluorescence spectroscopy [19], flow injection analysis [20], spectrofluorimetry and voltammetry method [21, 22]. The electroanalytical method is one of the powerful techniques for traces analysis with fast, high sensitivity, good precision and accuracy and low cost.



**Scheme 1.** Chemical structure of L-dopa.

To enhance the electron conductivity, we doped the nitrogen into graphene and decorated on nickel oxide, during this process the urea is employed to reduce the graphene oxide into N-doped graphene, which may have an excellent electron conductivity due to the combination of N into GE. Additionally, each N atom has  $\pi$  electron, which is only responsible for enhancing the electron conductivity. In our current study, nitrogen-doped graphene decorated with nickel oxide (N-GE/NiO) nanocomposite prepared and characterized by various analytical and spectroscopy technique. In addition, the as-synthesized nanocomposite useful as an L-dopa sensor, where the N-GE was used as the way for electron transfer, controlling the enlarging and loading space in the NiO.

## 2. EXPERIMENTAL SECTION

### 2.1. Chemicals

Graphite flakes (~105 mm flakes), sodium nitrate ( $\text{NaNO}_3$ ), potassium permanganate ( $\text{KMnO}_4$ ), sulphuric acid ( $\text{H}_2\text{SO}_4$ ), hydrochloric acid (10% HCl), hydrogen peroxide ( $\text{H}_2\text{O}_2$ ), urea ( $\text{CH}_4\text{N}_2\text{O}$ ), nickel oxide (NiO), ethanol ( $\text{C}_2\text{H}_6\text{O}$ ) were obtained from Shanghai Chemical Reagent Co., Ltd. Levodopa were purchased from Sigma Aldrich, Taiwan. All the chemicals, reagents and solvents were used for an analytical grade. Double distilled water was used whole experiments.

### 2.2. Characterizations

The crystalline structure of the N-GE/NiO composite was characterized by Powder X-ray diffraction (PXRD) by XPERT-PRO (PANalytical B.V., The Netherlands) diffractometer (Cu K $\alpha$  radiation,  $\lambda=1.54 \text{ \AA}$ ). Fourier-transform infrared (FT-IR) spectrum was recorded using a CHI 1000C FT-IR - 6600 spectrometers with a spectral resolution of  $2 \text{ cm}^{-1}$  using dry KBr pellet at ambient temperature. The Raman spectrum was documented at room temperature using a WITech CRM200

confocal microscopy Raman system with a 488 nm laser. Thermogravimetric analysis (TGA) measurements were performed using a Netzsch TG-209 series apparatus at a heating rate of  $10\text{ }^{\circ}\text{C min}^{-1}$  under a constant flow of nitrogen. The morphology and elemental composition of the as-prepared composite were studied by scanning electron microscopy (SEM Hitachi S-3000 H) attached with energy-dispersive X-ray analyzer, respectively. The chemical compositions and orientations of the grains were studied by transmission electron microscope (TEM) using a JEOL 2000 operating at 200 kV. Electrochemical performance was studied by using cyclic voltammetry (CHI 400 and CHI 900) techniques.

### 2.3. Preparation of N-GE/NiO composite

GO was prepared by the modified Hummers method [23]. Nickel oxide (1.6 mmol) mixed with GO solution (30 mg in 20 mL distilled water) and kept under continuous stirring for 1 h at a room temperature. Later, urea (10 mmol) dissolved in 10 mL water was added to the above solution drop by drop and placed on magnetic stirring for 60 min. The resulted mixture was transferred into a Teflon-lined autoclave with a stainless-steel shell, constant at  $180\text{ }^{\circ}\text{C}$  for 2 h. Consequently, the precipitate was washed with distilled water and ethanol. Then, it was dried at  $60\text{ }^{\circ}\text{C}$  under vacuum overnight. The above product was further calcinated in flowing argon atmosphere by heating at a rate of  $10\text{ }^{\circ}\text{C min}^{-1}$  from room temperature to  $400\text{ }^{\circ}\text{C}$  and maintained for 2 h to get the final composite [24].

## 3. RESULTS AND DISCUSSION

### 3.1. Structural properties

The XRD pattern of as-synthesized N-GE/NiO composite shown in Fig. 1A. The diffraction peak appeared at  $2\theta = 37.4^{\circ}$ ,  $43.2^{\circ}$ ,  $63.0^{\circ}$ , and  $75.2^{\circ}$  the corresponding planes are (111), (200), (220) and (311) are observed due to the NiO NPs and the broad diffraction peak observed at  $2\theta$  range between  $10$  to  $30^{\circ}$ , and its indicating amorphous nature of carbon-containing GE. In these results confirmed by the formation of N-GE/NiO composite. Which is good agreement and planes of cubic structure of as-synthesized composite (JCPDS # 047-1049). Fig. 1B shows that the FT-IR spectrum for N-GE/NiO composite. The strong absorption peak at  $579\text{ cm}^{-1}$  was characteristic of the metal oxygen of N-O peak. The peak at  $3576$  and  $1629\text{ cm}^{-1}$  can be attributed to the O-H mode of stretching and bending vibrations. Additionally, the sharp peak at  $1109$  and  $876\text{ cm}^{-1}$  corresponding to  $\text{CO}_2$  and  $\text{O}_2$  vibrations respectively. The strong peak at  $1109$  and  $876\text{ cm}^{-1}$  indicate the presence of N-GO coated on NiO nanoparticles.

Raman spectra of N-GE/NiO composite was shown in Fig. 1C. From this figure, there are five peaks observed at around  $200$ ,  $300$ ,  $550$ ,  $1100$  and  $1350\text{ cm}^{-1}$ , which is corresponding to 1P, 2P, 2P, G and D bands. The peak at  $1350\text{ cm}^{-1}$ , D band assigned to the  $\text{sp}^2$ -hybridized carbon atom of  $\text{E}_{2g}$  phonon mode and  $1100$  peak assigned stretching mode of Ni-O. The thermal stability of the N-GE/NiO composite was investigated using TGA analysis shown in Fig. 1D. TGA curve displays the so many

mass loss of thermal decomposition. The Fig. 1D shows the first weight loss occurs from 100 to 400 °C, which is around the boiling or decomposition point of physically absorbed water molecules, and impurities. The second peak appeared at 400 °C and then slightly oxidation of the NiO, after that the weight loss is gradually increased with increasing the temperature, which indicates the loss of weight confirm the strong binding between the N-GE and NiO NPs. Fig. 1 (E and F) shows the FE-SEM and TEM image of N-GE/NiO composite. Fig. 1 (E) composite agglomerated and NiO NPs has uniformly distributed with the surface on N-GE sheet edge. EDX spectrum of the as-prepared composite is inset in Fig. 1 (E). Fig. 1 (F) shows the TEM image of the composite with different magnification and the result shows, NiO composite has homogeneously dispersed surface on N-GE.

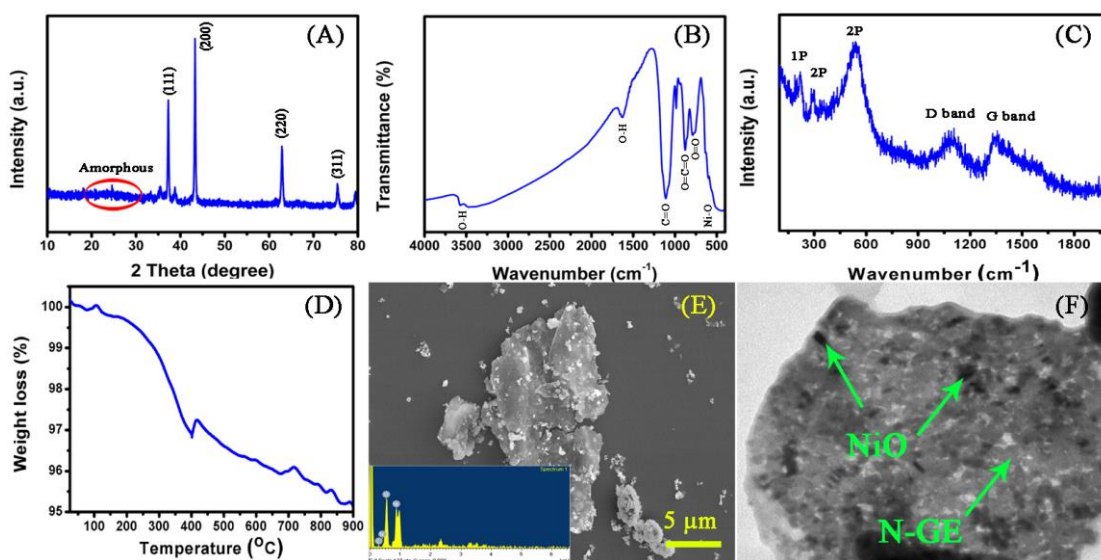


**Figure 1.** (A) XRD, (B) FT-IR, (C) Raman, (D) TGA, (E) FE-SEM and (F) TEM images of N-GE/NiO composite.

### 3.2. Electrochemical performance

Fig. 2 shows that the electrocatalytic activity of GCE modified CVs obtained (a) bare GCE (b) NiO (c) GO and (d) N-GE/NiO/GCE modified electrodes with 200  $\mu\text{M}$  L-dopa in PBS solution at the scanning rate of  $50 \text{ mV s}^{-1}$ . In Fig. 2, bare GCE (a), NiO (b), GO (c) does not show any significant response for the electrochemical detection of L-dopa with the peak potential of 0.436, 0.292, 0.394 V, which is observed due to the poor catalytic activity. Afterwards, there is a commendable response occurred for N-GE/NiO/GCE (d) higher peak potential at 0.09 V demonstrates that the low potential has the higher electron transfer capacity. Additionally, the oxidation peak current of L-dopa was much more occurred for N-GE/NiO/GCE than the bare GCE, NiO and GO. In these results, the electrochemical behavior of L-dopa has an irreversible two protons and two electrons transfer at the oxidation-oxidation process [19]. The oxidation mechanism of L-dopa is shown in Scheme 2.

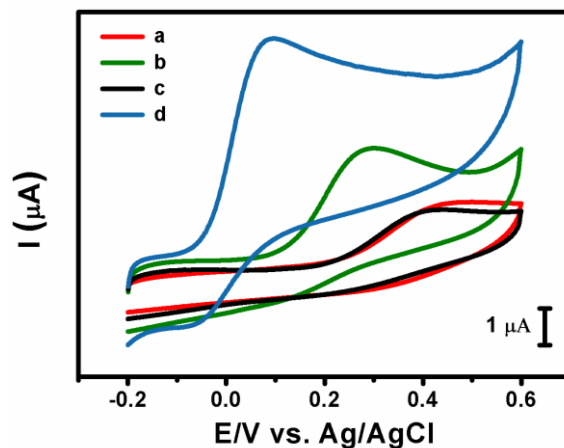
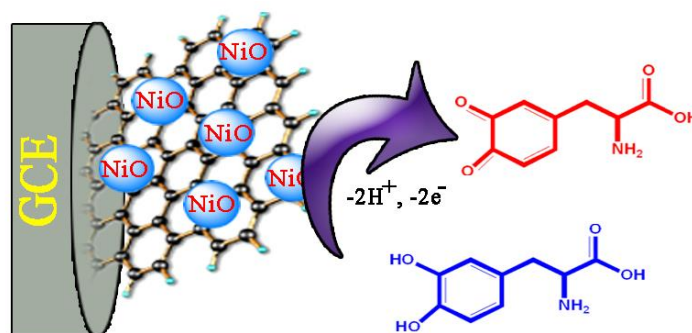


**Figure 2.** CV response of (a) bare GCE presence of L-dopa, (b) NiO (c) GO (d) N-GE/NiO/GCE with 200  $\mu\text{M}$  L-dopa in 0.05 M PBS (pH 7). Scan rate: 50  $\text{mV s}^{-1}$ .



**Scheme 2.** Oxidation mechanism of L-dopa.

### 3.3. Effect of concentrations and scanning rates

Fig. 3A reveals that the CV responses of N-GE/NiO/GCE in PBS (pH 7) containing different concentrations of L-dopa at a scanning rate 50  $\text{mV s}^{-1}$ . When the absence of L-dopa (a), the N-GE/NiO/GCE does not appear any distinct peaks. For the meantime, the oxidation peak was observed after the addition of 100  $\mu\text{M}$  L-dopa. Then, the oxidation peak current increases gradually with increasing the L-dopa concentrations from 100 to 1000  $\mu\text{M}$  L-dopa. The results showed that the excellent electro-oxidation behavior of L-dopa at N-GE/NiO/GCE and can be used for sensitive determination of L-dopa. Fig. 3B determines the plot between oxidation peak current and L-dopa concentrations, which may be interconnected by a linear regression equation as  $E_{\text{pa}} (\text{V}) = 26.87x - 1.432$ ,  $R^2 = 0.9972$ .

Fig. 3C represents that the effect of scanning rate of electro-oxidation responses of N-GE/NiO/GCE in PBS with L-dopa. The steady increase in oxidation peak current while increasing the anodic peaks from 20 to 200  $\text{mV s}^{-1}$  is experimental in CV curve. When the oxidation peaks current ( $I_{\text{pa}}$ ) increases the square root of the scan rate also increases linearly. Additionally, the inset linear plot among oxidation peak current versus the square root of the scan rates has displayed a relationship

which suggesting that the oxidation process of L-dopa appeared at the N-GE/NiO/GCE is a diffusion-controlled electron transfer process Fig. 3D [12]. From the results, we approve that the observed CV reports are due to the determination of L-dopa diffused on the surface of the N-GE/NiO/GCE. Fig. 3D demonstrates the plot between oxidation peak current and the square root of scan rate, which may be communicated by a linear regression equation as  $E_{pa} (V) = 0.5824x - 0.537$ ,  $R^2 = 0.9933$  [25-29].

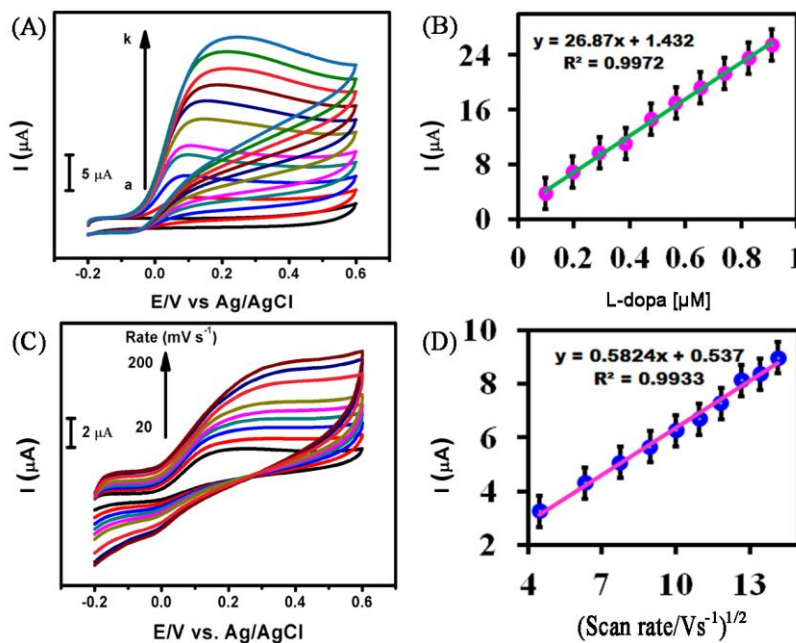


**Figure 3.** CV response of N-GE/NiO/GCE (A) Different concentrations of L-dopa (a = absence; b-k = 100-1000  $\mu\text{M}$  L-dopa) Scan rate:  $50 \text{ mV s}^{-1}$ , (B) plot of oxidation peak current versus the concentration of L-dopa, (C) different scan rates of  $200 \mu\text{M}$  L-dopa from 20 to  $200 \text{ mV s}^{-1}$  and (D) plot of oxidation peak current versus the square root of the scan rates.

### 3.4. Calibration plot and limit of detection

Differential pulse voltammetry was achieved to examine the relationship between the concentration of L-dopa and peak current owing to its high sensitivity. As can be seen in Fig. 4A, under the optimum conditions, the oxidation peak current was relational to L-dopa concentration in the range from 0.03 to  $386.8 \mu\text{M}$  with the regression equation of  $I_{pa} (A) = 3.2564x + 1.1476$  and  $R^2 = 0.996$ . The detection limit was  $17 \text{ nM}$  ( $S/N = 3$ ). However, the linear range (Fig. 4 B) obtained in this work is (0.03 –  $386.8 \mu\text{M}$ ). The calibration curves of L-dopa at N-GE/NiO/GCE were also investigated. The linear ranges for N-GE/NiO/GCE were from 0.03 to  $386.8 \mu\text{M}$ . The corresponding detection limits were  $0.017 \mu\text{M}$  ( $S/N = 3$ ). The wide linear range and the low detection limit can be attributed to the immobilization of nitrogen-doped graphene on the GCE surface with satisfied surface area and conductivity. The similarity of analytical parameters like as limit of detection, and linear range of L-dopa compared to previous reports (Table 1). It is evident that this sensor exhibited higher catalytic activity towards L-dopa with a least LOD and good linear range than the other modified electrodes.

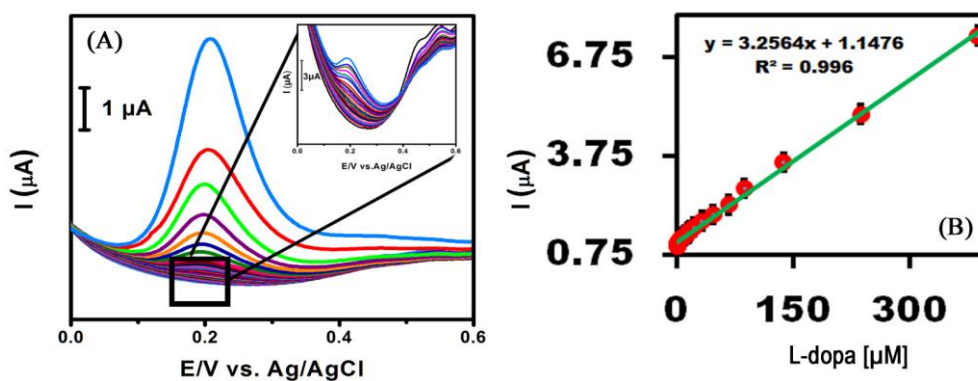


**Figure 4.** DPVs of N-GE/NiO/GCE (A) increasing L-dopa concentration (0.03–386.8  $\mu\text{M}$ ), (B) calibration curve of the peak currents on the L-dopa concentrations and (C) calibration curve of the peak currents on the L-dopa. Scan rate:  $50 \text{ mV s}^{-1}$ .

**Table 1.** Comparison of analytical parameters such as limit of detection and linear range of L-dopa with previous reports.

Electrode	Modifier	Method	pH	Linear Range ( $\mu\text{M}$ )	LOD ( $\mu\text{M}$ )	Ref
CPE	PbO <sub>2</sub>	DPV	7	260-1200	25	30
PGE	AuNP-CNT	DPV	7	0.1-150	0.005	31
GCE	SW-CNT	DPV	5	0.5-20	0.3	32
CPE	Ru-red/Nay	CV	4.8	120-0.01 Mol/ L	85	33
GCE	P-Ni <sup>II</sup> TAPC	IT	4	10-0.1	0.1	34
GCE	ppy-CNT	DPV	7	1.0-100	0.1	35
GPE	Oxavanadium-Salen	IT	6	1.0-100	0.8	36
SPCE	Activated SPCE	CV	2.21	1.0-100	0.47	37
GCE	Ferrocene	DPV	7	2-500	1.2	38
CPE	Poly(methyl orange) film	DPV	5	10-800	3.69	39
GCE	Graphene	DPV	6.2	0.04-79	0.022	40
CPE	Dysprosium nanowire	FFT-SWV	7	0.01-1	0.004	41
GCE	TNF/GO	DPV	6	0.3-60	0.0159	42
CPE	MBICl/NiO/NPs	DPV	6	0.7-900	0.4	43
<b>GCE</b>	<b>N-GE/NiO</b>	<b>DPV</b>	<b>7.0</b>	<b>0.03 – 386.8</b>	<b>0.017</b>	<b>This work</b>

### 3.5. Selectivity

The selectivity of the proposed sensor was observed by DPV in the presence of 10-fold excess concentrations of mercury ( $\text{Hg}^{2+}$ ), sodium ( $\text{Na}^{2+}$ ), potassium ( $\text{K}^+$ ), calcium ( $\text{Ca}^{2+}$ ), zinc ( $\text{Zn}^{2+}$ ), chromium ( $\text{Cr}^{2+}$ ), lead ( $\text{Pb}^{2+}$ ), glucose (Glu), uric acid (UA), ascorbic acid (AA), dopamine (DA) L-cysteine (L-Cys) and acetaminophen (AC) and the found results are shown in Fig. 5. The experimental conditions for selectivity studies are same as of in Fig. 4. Fig. 5 clearly shows that the  $\text{Hg}^{2+}$ ,  $\text{Na}^{2+}$ ,  $\text{K}^+$ ,  $\text{Ca}^{2+}$ ,  $\text{Zn}^{2+}$ ,  $\text{Cr}^{2+}$ ,  $\text{Pb}^{2+}$ , Glu, DA, and AA did not display any noticeable answer at N-GE/NiO/GCE; while UA, AC, and L-Cys displayed a minor response at the potential of 0.207 V. Though, Glu, AA, Ac and L-Cys did not interrupt the oxidation peak potential of L-dopa, whereas a small shift in the cathode peak potential was detected in presence of UA. The results obviously show that the selectivity effect of Glu, AA, AC, and L-Cys is irrelevant for the detection of L-dopa at N-GE/NiO/GCE. The result specifies that the worthy selectivity of the modified sensor.

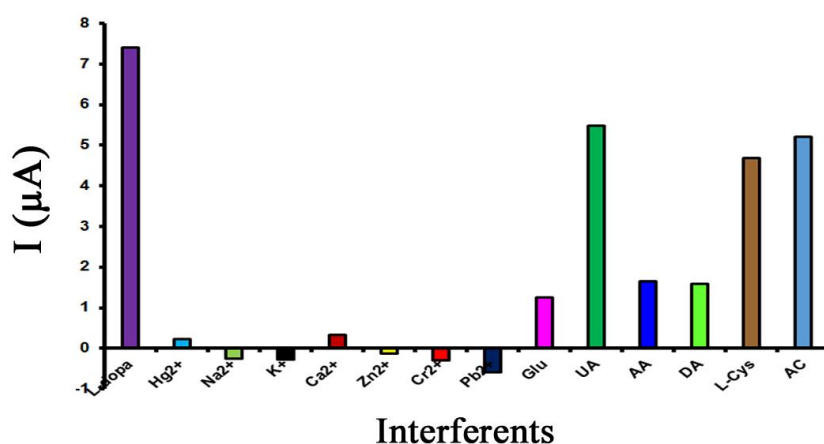


**Figure 5.** Variation in DPV current response (%) of N-GE/NiO/GCE for L-dopa in the presence of additions of different metals and biological compounds. Scan rate:  $50 \text{ mV s}^{-1}$ .

### 3.6. Accumulation time, reproducibility and operational stability

Fig. 6 shows that the accumulation time study. In this figure, the oxidation peak current of L-dopa were recorded for the different accumulation time started from 0 to 300 s. The oxidation peaks current of L-dopa increases with the increase of accumulation time. The highest oxidation peak current was recorded at 150 s. Hence, the optimized accumulation time of 150 s was adopted for the efficient oxidation of L-dopa. In order to study the reproducibility of the sensor, five different N-GE/NiO/GCE were verified for the discovery of  $200 \mu\text{M}$  L-dopa in PBS solution at the scanning rate of  $50 \text{ mV s}^{-1}$ . The reproducibility results are shown in Fig. 6. From this results, N-GE/NiO/GCE having an excellent reproducible capacity to detect L-dopa. The CV replies of 50 consecutive cycles of the N-GE/NiO/GCE both presence and absence of L-dopa in  $200 \mu\text{M}$  is shown in Fig. 6 C and D This result proves that the modified electrode having a great operational stability for the above 50 consecutive cycles.

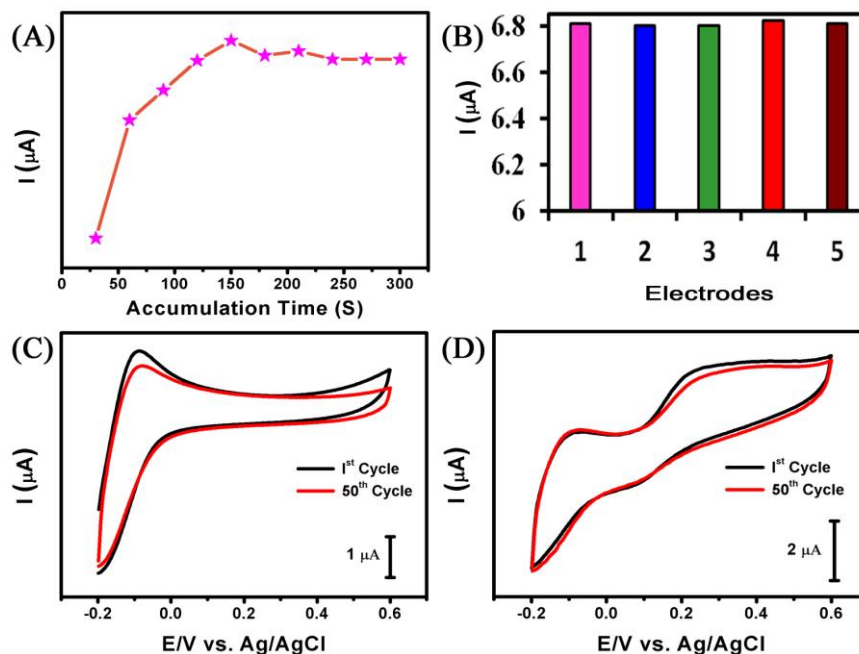


**Figure 6.** CVs obtained at (A) accumulation time (B) reproducibility and operational stability of the N-GE/NiO/GCE (C) without (D) with L-dopa.

### 3.7. Real sample analysis

The suggested L-dopa sensor was extra tested using real sample analysis, such as a sweet potato (*Ipomoea batatas*) were obtained from a local market in Taipei, Taiwan (ROC). The extracted juice was ultra-centrifuged prior to the real sample studies. The juice extract was spiked by L-dopa in PBS solution (10 mL), as shown in Fig. 7. Obviously, the fabricated electrode is absolutely suitable for real sample analysis, the corresponding DPV results are shown in Fig. 7 and Table 2.

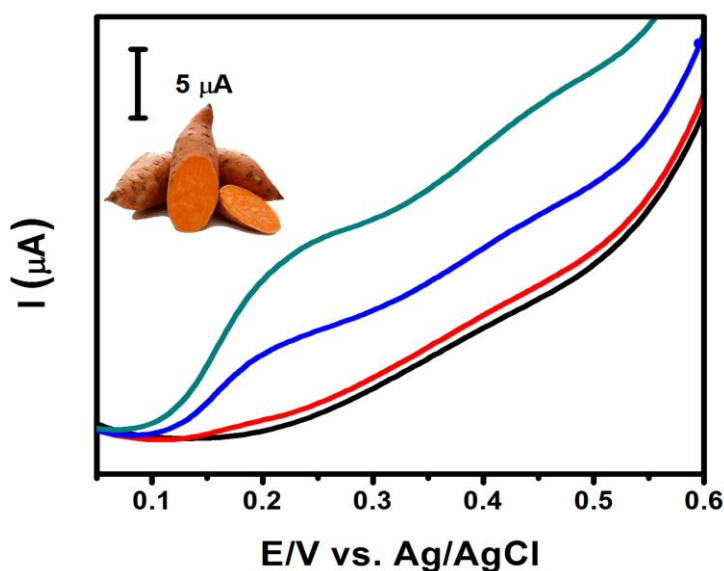


**Figure 7.** DPVs of the N-GE/NiO/GCE in sweet potato juice sample spiked by L-dopa with PBS (pH 7). Scan rate:  $50 \text{ mV s}^{-1}$ .

**Table 2.** Real sample analysis of L-dopa using spiked method N-GE/NiO/GCE. (n = 3)

S.No	Vegetable Sample	Added ( $\mu\text{M}$ )	Found ( $\mu\text{M}$ )	Recovery (%)	RSD (%)
1	Sweet potato	10	9.78	97.8	2.36
		20	21.35	101.5	3.25
		30	30.14	101.01	2.86

RSD = Relative standard deviation.

#### 4. CONCLUSIONS

In conclusion, N-GE/NiO nanocomposite is prepared and studied by PXRD, FT-IR, Raman, TGA, FE-SEM, TEM and electrochemical methods such as CV and DPV. The electro-oxidation behavior, electrochemical property, and influence of scan rates were studied. The proposed method was applied for the detection of L-dopa in the vegetable sample. The N-GE/NiO nanocomposite platform gives a fast response repeatability, fast response, low detection limit, good stability and good potential applications toward the detection of L-dopa. Further, selective determination of L-dopa was also achieved by this proposed sensor in the presence of common interferents like as glucose, urea, and ascorbic acid.

#### ACKNOWLEDGMENTS

The authors gratefully acknowledge the financial support of the National Taipei University of Technology, and Mackay Memorial Hospital Joint Research Program (NTUT-MMH-No.107-01). The National Science Council, and The Ministry of Education, Taiwan supported this work. We would also like to acknowledge The Ministry of Science and Technology, Taiwan (MOST106-2221-E-182-021 and MOST 106-2113-M-027-003) and MacKay Memorial Hospital, Taipei, Taiwan (MMH-TT-10701) for their financial support.

#### References

- H. M. Hegab, A. ElMekawy, B. van den Akker, M. Ginic-Markovic, C. Saint, G. Newcombe and D. Pant, *Reviews in Environ. Sci. Technol.*, (2018) 1.
- H. J. Shin, K.K. Kim, A. Benayad, S.M. Yoon, H.K. Park, I.S. Jung, M.H. Jin, H.K. Jeong, J.M. Kim and J.Y. Choi, *Adv. Funct. Mater.*, 19 (2009) 1987.
- Z. Lei, L. Lu and X. Zhao, *Energy Environ. Sci.*, 5 (2012) 6391.
- M. Fouladgar, H. Karimi-Maleh and V.K. Gupta, *J. Mol. Liq.*, 208 (2015) 78.
- Y. Misu, H. Ueda and Y. Goshima, *Elsevier*, (1995) 427.
- M.Z. Ahmad, K.A. Hamid and T.J.B. Effendi, *2012 IEEE Symposium on, IEEE*, (2012) 134.
- A. Alexandra Rabinca, M. Buleandra, F. Tache, C. Mihailciuc, A. Magdalena Ciobanu, D. Cristian Stefanescu and A. Alexandru Ciucu, *Curr. Anal. Chem.*, 13 (2017) 218.
- S.N. Alam, N. Sharma and L. Kumar, *Graphene*, 6 (2017) 1.
- X. Feng, J. Zhou, L. Wang, Y. Li, Z. Huang, S. Chen, Y. Ma, L. Wang and X. Yan, *New J. Chem.*, 39 (2015) 4026.
- M.-C. LI, H.-F. WU, J.-Q. HU and C.-A. MA, *Acta Phys. Chim. Sin.*, 24 (2008) 1937.

11. M. Marin, C. Lete, B.N. Manolescu and S. Lupu, *J. Electroanal Chem.*, 729 (2014) 128.
12. M.F. Teixeira, L. Marcolino-Junior, O. Fatibello-Filho and E. Dockal, M.F. Bergamini, *Sens. Actuator B-Chem.*, 122 (2007) 549.
13. S. Shahrokhian and E. Asadian, *J Electroanal Chem*, 636 (2009) 40.
14. A. Sivanesan and S.A. John, *Biosens. Bioelectron.* , 23 (2007) 708.
15. P. Prabhu, R.S. Babu and S.S. Narayanan, *Sens. Actuator B-Chem.*, 156 (2011) 606.
16. H.C.d. Melo, A.P.D. Selegim, W.L. Polito, O. Fatibello-Filho and I.C. Vieira, *J. Braz. Chem. Soc.* , 18 (2007) 797.
17. G. Hu, L. Chen, Y. Guo, X. Wang and S. Shao, *Electrochim. Acta* , 55 (2010) 4711.
18. S. Hu, C. Xu, G. Wang and D. Cui, *Talanta*, 54 (2001) 115.
19. X.-X. Yan, D.-W. Pang, Z.-X. Lu, J.-Q. Lü and H. Tong, *J. Electroanal Chem*, 569 (2004) 47.
20. M. El Mhammedi, M. Achak, M. Bakasse and A. Chtaini, *J. Hazard. Mater.* , 163 (2009) 323.
21. O. Corduneanu, M. Garnett and A.M.O. Brett, *Anal. Lett.* , 40 (2007) 1763.
22. M.F. Teixeira, M.F. Bergamini, C.M. Marques and N. Bocchi, *Talanta*, 63 (2004) 1083.
23. W.-D. Zhang, J. Chen, L.-C. Jiang, Y.-X. Yu and J.-Q. Zhang, *Microchim. Acta*, 168 (2010) 259.
24. G. Wang, X. Lu, T. Zhai, Y. Ling, H. Wang, Y. Tong and Y. Li, *Nanoscale*, 4 (2012) 3123.
25. F. Cao, S. Guo, H. Ma, D. Shan, S. Yang and J. Gong, *Biosens. Bioelectron.* , 26 (2011) 2756.
26. Y. Mu, D. Jia, Y. He, Y. Miao and H.-L. Wu, *Biosens. Bioelectron.* , 26 (2011) 2948.
27. E. Nalewajko, A. Wiszowata and A. Kojło, *J. Pharm. Biomed. Anal.* , 43 (2007) 1673.
28. R. Gangopadhyay and A. De, *Chem. Mater.* , 12 (2000) 608.
29. Y. Qiu, X. Zhang and S. Yang, *Phys. Chem. Chem. Phys.* , 13 (2011) 12554.
30. H. C. D . Melo, A. P. D. Selegim, W. L. Polito, O. Fatibello-Filho and I. C. Vieira, *J. Braz. Chem. Soc.* , 18 (4) (2007) 797.
31. G. Hu, L. Chen, Y. Guo, X. Wang and S. Shao, *Electrochim. Acta*, 55 (16) (2010) 4711.
32. X. -X. Yan, D. -W. Pang, Z. -X. Lu, J. -Q. Lü and H. Tong, *J. Electroanal Chem.* , 569 (1) (2004) 47.
33. M. F. Teixeira, M. F. Bergamini, C. M. Marques and N. Bocchi, *Talanta*, 63 (4) (2004) 1083.
34. A. Sivanesan and S. A. John, *Biosens. Bioelectron.* , 23 (5) (2007) 708.
35. S. Shahrokhian and Asadian, *J. Electroanal Chem.*, 636 (1) (2009) 40.
36. M. F. Teixeira, L. Marcolino-Junior, O. Fatibello-Filho, E. Dockal and M. F. Bergamini, *Sens. Actuator B-Chem.* , 122 (2) (2007) 549.
37. A. Alexandra Rabinca, M. Buleandra, F. Tache, C. Mihailciuc, A. Magdalena Ciobanu, D. Cristian Stefanescu and A. Alexandru Ciucu, *Curr. Anal. Chem.*, 13 (3) (2017) 218.
38. H. Yaghoobian, H. Karimi-Maleh, M. A. Khalilzadeh and F. Karimi, *Int. J. Electrochem. Sci* 4 (7) (2009) 993.
39. K. Reddaiah, T. M. Reddy and P. Raghu, *J. Electroanal Chem.* , 682 (2012) 164.
40. M. Arvand and N. Ghodsi, *J. Solid State Electrochem.* , 17 (3) (2013) 775.
41. P. Daneshgar, P. Norouzi, M. R. Ganjali, R. Dinarvand and A. A. Moosavi-Movahedi, *Sensors* 9 (10) (2009) 7903.
42. M. Arvand and N. Ghodsi, *Sens. Actuator B-Chem.* , 204 (2014) 393.